Supporting Information

Plasma-catalytic One-step Steam Reforming of Methane to Methanol: Revealing the Catalytic Cycle on Cu/MOR

Yingzi Hao,[1, #] Shangkun Li,[2 #] Wei Fang,[1] Ximiao Wang,[1] Zhaolun Cui,[3] Kristof M. Bal,[2] Nick Gerrits,[2] Hongchen Guo,[1] Erik C. Neyts,[2] Annemie Bogaerts,[2] Yanhui Yi [1]*

[1]State Key Laboratory of Fine Chemicals, Frontier Science Center for Smart Materials, School of Chemical Engineering, Dalian University of Technology, Dalian 116024, P.R. China.

[2]Research group PLASMANT, Department of Chemistry, University of Antwerp, Universiteitsplein 1, BE-2610 Wilrijk-Antwerp, Belgium.

[3]School of Electric Power Engineering, South China University of Technology, Guangzhou 510630, China.

Table of Contents

S1. Calculation of conversion, product selectivity and energy efficiency

To evaluate the reaction performance of the catalyst, the conversion of the reactants and the selectivity of the main products were calculated by the following equations. All product concentrations were obtained by standard curves.

The CH_4 conversion was calculated by:

$$X_{CH_4}(\%) = \frac{n_{CH_4}^{inlet} - n_{CH_4}^{outlet}}{n_{CH_4}^{inlet}} \times 100\% \quad \text{(S1)}$$

Where X represents the gas conversion, n represents the moles of reactants or products.

The selectivity of the gaseous products was calculated as：

$$S_{C_2H_6}(\%) = \frac{2n_{C_2H_6}^{outlet}}{n_{CH_4}^{inlet} - n_{CH_4}^{outlet}} \times 100\% \quad \text{(S2)}$$

$$S_{C_2H_4}(\%) = \frac{2n_{C_2H_4}^{outlet}}{n_{CH_4}^{inlet} - n_{CH_4}^{outlet}} \times 100\% \quad \text{(S3)}$$

$$S_{C_3H_6}(\%) = \frac{3n_{C_3H_6}^{outlet}}{n_{CH_4}^{inlet} - n_{CH_4}^{outlet}} \times 100\% \quad \text{(S4)}$$

$$S_{CO}(\%) = \frac{n_{CO}^{outlet}}{n_{CH_4}^{inlet} - n_{CH_4}^{outlet}} \times 100\% \quad \text{(S5)}$$

$$Sco_2(\%) = \frac{n_{co_2}^{outlet}}{n_{CH_4}^{inlet} - n_{CH_4}^{outlet}} \times 100\% \quad \text{(S6)}$$

The selectivity of the liquid products was calculated as follows:

$$\text{Total selectivity of liquid product}(\%) = 100\% - (S_{C_2H_6} + S_{C_2H_4} + S_{C_3H_6} + S_{CO} + Sco_2) \quad \text{(S7)}$$

$$S_{C_xH_yO_Z}(\%) = \frac{xn_{C_xH_yO_Z}}{n_{CH_3OH} + 2n_{C_2H_5OH} + 2n_{CH_3CHO} + 2n_{CH_3COOH}} \times \text{Total selectivity of liquid product}(\%) \quad \text{(S8)}$$

Where $n_{C_xH_yO_z}$ represents the number of moles of various oxygenates in the liquid fraction. Note that equation (S9) is only valid when the amount of coking is negligible, which is the case in our experiments. Additionally, we estimate the H_2O conversion (S10) based on the oxygen balance, and then we calculate the H_2 selectivity (S11).

$$X_{H_2O}(\%) = \frac{n_{CO}^{outlet} + 2n_{CO_2}^{outlet} + z \times n_{n\,C_xH_yO_z}^{outlet}}{n_{H_2O}^{inlet}} \times 100\% \quad \text{(S9)}$$

$$S_{H_2}(\%) = \frac{n_{H_2}^{outlet}}{2 \times n_{CH_4}^{inlet} \times X_{CH_4} + n_{H_2O}^{inlet} \times X_{H_2O}} \times 100\% \quad \text{(S10)}$$

The energy consumption for the production of CH_3OH was defined as follows:

$$\text{Energy consumption (kJ/mmol)} = \frac{\text{discharge power (kJ/s)}}{\text{rate of } CH_3OH \text{ produced (mmol/s)}} \quad \text{(S11)}$$

Table S1. Standard curve formula of all substances in the system

Products	Equation	Adj. R-Square
CH_4	$Y=3.96820507*10^6*X + 65036.71$	0.999
C_2H_6	$Y =7.4515*10^6*X$	0.999
C_2H_4	$Y =7.55518*10^6*X$	0.999
C_3H_6	$Y =1.6011374*10^7*X$	0.998
CO	$Y =1.04671*10^7* X$	0.998
CH_3OH	$Y=9.27044*10^4*X$	0.998
C_2H_5OH	$Y=1.18790*10^5*X$	0.999
CH_3CHO	$Y=2.96785*10^4*X$	0.998
CH_3COOH	$Y=4.96131*10^4*X$	0.999

X represents the concentration of liquid sample (mol/L); Y represents the peak area of the sample.

S2. Liquid products: Qualitative analysis

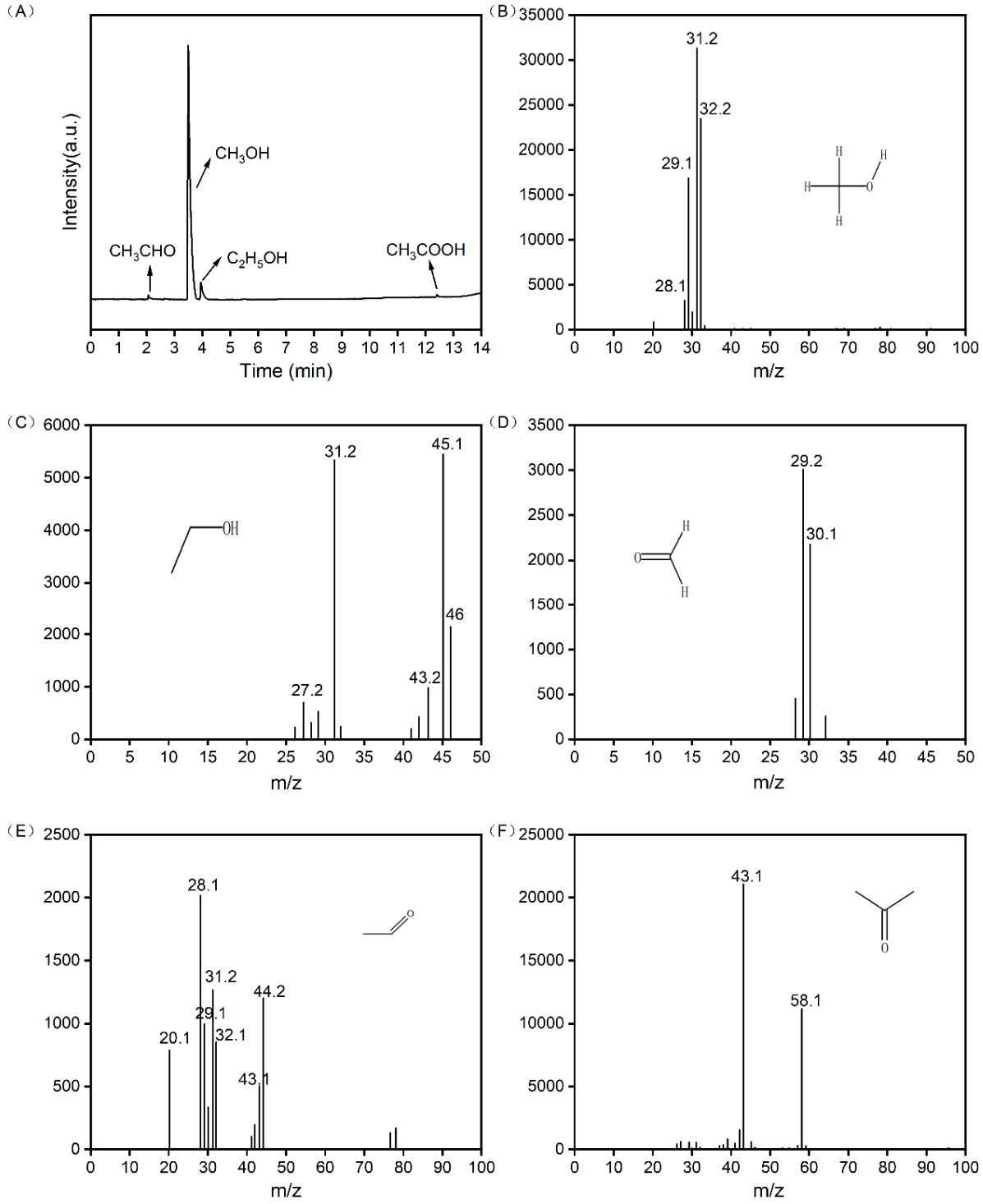

Figure S1. Results of qualitative analysis of liquid products. (A) Gas chromatography, indicating the presence of CH_3OH, C_2H_5OH, CH_3CHO and CH_3COOH. GC-MS analysis results. (B) Methanol; (C) Ethanol; (D) Formaldehyde; (E) Acetaldehyde; (F) Acetone. Note that acetone is the wash solution, resulting in higher acetone abundance in the GC-MS results than the actual amount produced.

The liquid products were qualitatively analyzed by gas chromatography (GC) and gas chromatography mass spectrometry (GC-MS), as shown in Figure S1. GC results (Figure S1A) show the presence of CH_3OH, C_2H_5OH, CH_3CHO and CH_3COOH. We used the external standard method to quantify the liquid products. In addition, the MS signals of methanol, ethanol, formaldehyde, and acetaldehyde are listed in Figure S1B – S1E. Note that acetone (S1F) is the wash solution, resulting in higher acetone abundance in the GC-MS results. In summary, the liquid products mainly include CH_3OH, HCHO, C_2H_5OH, CH_3CHO and CH_3COOH by qualitative analysis of GC and GC-MS.

S3. Optimization of reaction conditions

The temperature (Figure S2A) and CH_4/H_2O ratio (Figure S2B) have been tested with Cu/MOR catalyst on plasma-catalytic OSRMtM. The CH_4 conversion increased with temperature from 130 °C to 290 °C, but the CH_3OH selectivity reached a peak at 170 °C. In order to maximize the CH_3OH production, we continued our experiments at 170 °C. By investigating different CH_4/H_2O ratios, an optimal CH_4/H_2O ratio was 1:4, with 77 % CH_3OH selectivity was found. Therefore, we study the plasma-catalytic OSRMtM reaction performance and the mechanisms under the optimized reaction conditions (170 °C; CH_4/H_2O ratio = 1:4).

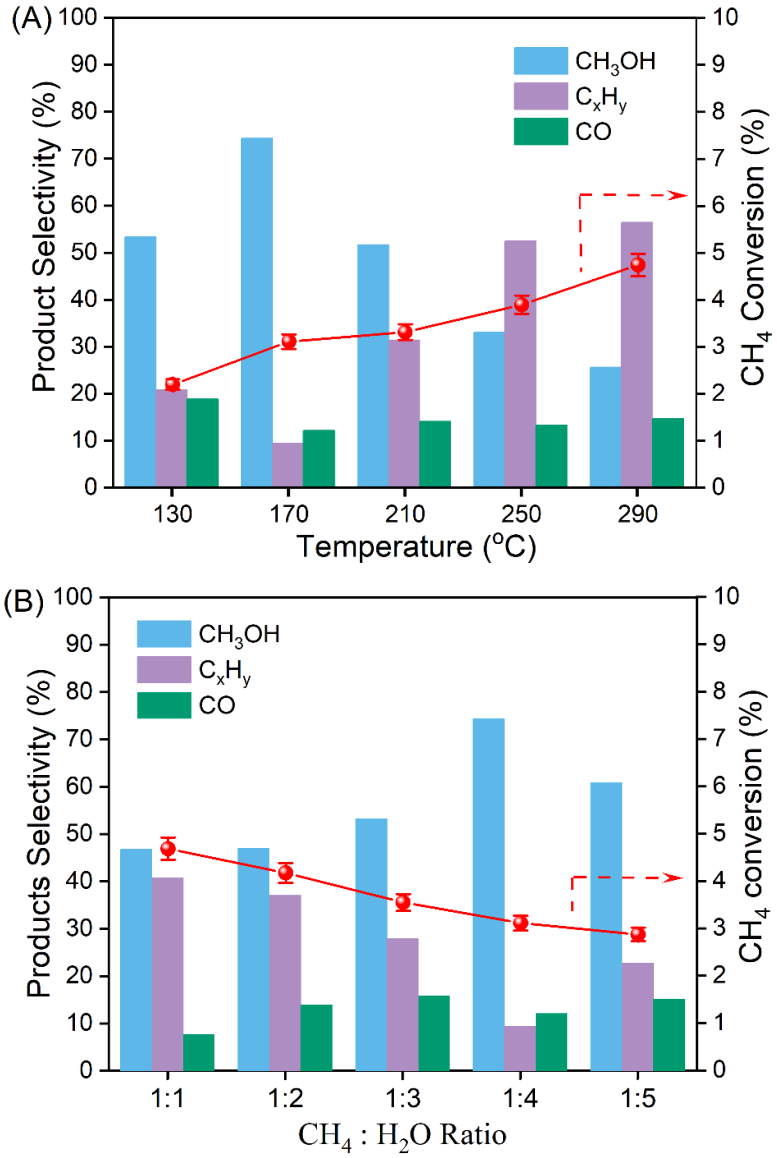

Figure S2. Experimental results of OSRMtM with Cu/MOR, varying (A) temperature and (B) the ratio of CH_4 and H_2O. Reaction conditions: 1.7 wt.% Cu loading; discharge length: 5 cm; discharge power: 7 W; total flow rate: 100 ml/min.

S4. Energy consumption at different conditions

The discharge voltage and current were measured by a digital fluorescence oscilloscope (Tektronix, DPO 3012) with a high voltage probe (Tektronix P6015) and a current probe (Pearson 6585) to obtain the Lissajous figures, which were used to calculate the plasma power and monitor the discharge properties. As shown in Figure S3, packing Cu/MOR catalyst can slightly reduce the discharge power compared to MOR catalyst. The energy consumption for CH_3OH production through plasma-catalytic OSRMtM by the Cu/MOR catalyst is (only) 22.7 kJ/mmol (Figure S3), which is much lower than with plasma only (79.7 kJ/mmol) and plasma + MOR (114.3 kJ/mmol).

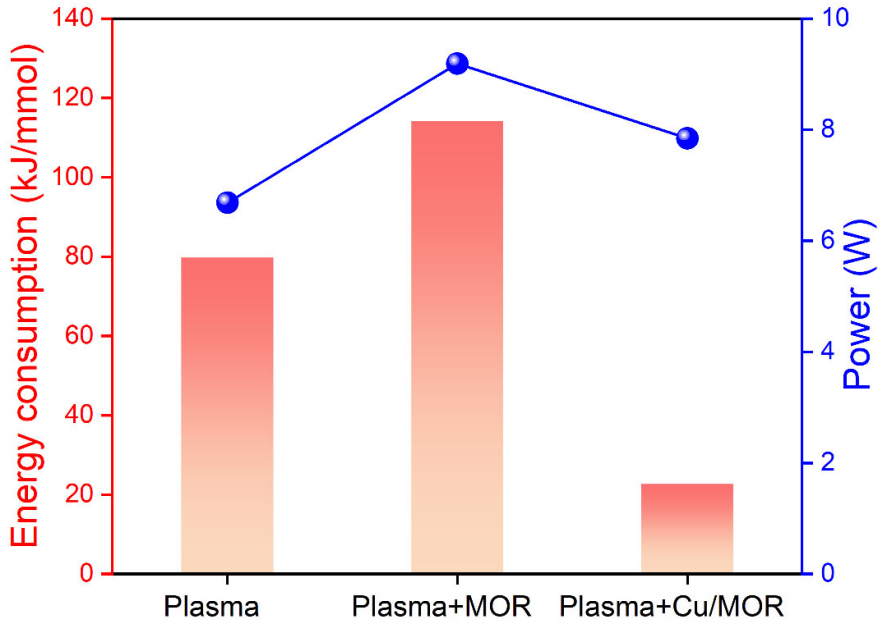

Figure S3. Energy consumption for CH_3OH production, and discharge power, for plasma only, plasma + MOR, and plasma + Cu/MOR at 443 K.

S5. Comparison of this work with literature results with H_2O as oxidant

Table S2. Summary of plasma catalysis and thermal catalysis for OSRMtM performance.

Plasma catalysis in this paper			
Catalyst	**Conditions**	**CH_4 conversion (%)**	**CH_3OH selectivity (%)**
MOR	170 °C; 1 bar	2.0	26.7
Cu-MOR IE1		2.4	51.8
Cu/MOR IE2		3.0	70.9
Cu/MOR IE3		2.9	70.7
Cu/MOR IE4		3.0	77.0
Cu/MOR IE5		3.0	71.5

Thermal catalysis from literature				
Catalyst	**Conditions**	**CH_4 conversion (%)**	**CH_3OH selectivity (%)**	**CH_3OH yield (mmol/mol_{Cu} /h)**
Cu-H-MOR [1]	350 °C	0.001335	100%	20.8±2.6
Cu-SSZ-13 [2]	225 °C	0.000187	~	12.7±0.4
Cu-CHA [3]	300°C	0.0136	91%	543
Cu-MOR [4]	350 °C	~	~	33
Cu/MOR [5]	200 °C	0.106	97%	0.41
Cu/MOR [6]	200 °C	0.072	98%	0.37

Plasma and plasma catalysis from literature			
Catalyst	**Conditions**	**CH_4 conversion (%)**	**CH_3OH selectivity (%)**
Plasma only [7]	CH_4: H_2O=1:1; 3 W	5	20
Plasma only [8]	CH_4: H_2O=1:5; 120°C	1.07	7.5
Plasma + TiO_2 [9]	35 °C; 1 bar; 30 W	~	93 (only in liquid phase)
Plasma + Cu/MOR [10]	120 °C; 1 bar; 30 W	~ 3	< 30 (86 only in the liquid phase)

In order to estimate the difference in performance between plasma catalysis and thermal catalysis, we calculate the CH_4 conversion based on the corresponding reference results by equation (S12). The CH_4 flow rate was converted to standard conditions (25 °C, 1 bar). As shown in Table S2, the difference in the reaction conditions result in the orders of magnitude differences in CH_4 conversion in thermal catalysis mainly due to the multi-step catalytic cycle reactions, i.e., a non-continuous process.

$$X_{CH_4}(\%) = \frac{Y_{CH3OH}/S_{CH3OH}}{n_{CH4}} \times 100\% \qquad \text{(S12)}$$

S6. Physicochemical properties of Cu/MOR catalysts

Table S3. Physicochemical properties of Cu/MOR catalysts.

Catalyst	Si/Al ratio	Cu/Al ratio	Cu loading (wt.%)	S_{BET} (m^2g^{-1})	V_{micro} (cm^3g^{-1})	Pore Size （nm）
MOR	17.0	0.000	0.000	596.0	0.216	1.668
Cu/MOR IE-1	17.8	0.10	0.94	543.4	0.195	1.700
Cu/MOR IE-2	18.2	0.15	1.34	521.1	0..187	1.690
Cu/MOR IE-3	18.5	0.16	1.52	531.7	0.191	1.717
Cu/MOR IE-4	18.6	0.20	1.78	521.0	0.191	1.632
Cu/MOR IE-5	18.5	0.21	1.96	453.6	0.167	1.649

N_2-physisorption was performed at -196 °C on a Micromeritics ASAP 2020 instrument to obtain structural information. Prior to the measurements, the samples were degassed under vacuum at 400 °C for 6 hours. The surface area was calculated by the Brunauer, Emmett and Teller (BET) method and the pore volume was obtained by the t-plot method. As shown in Table S3 and Figure S4, there is no evident change on the surface area, average pore size and pore volume of the Cu/MOR catalysts with four times Cu exchange. However, the surface area significantly decreased after five times change, indicating larger Cu clusters agglomeration on the MOR support. According to the IUPAC classification, all isotherms in Figure S4 belong to type I curves, which are typical for microporous materials.

S7. Nitrogen adsorption-desorption isotherms

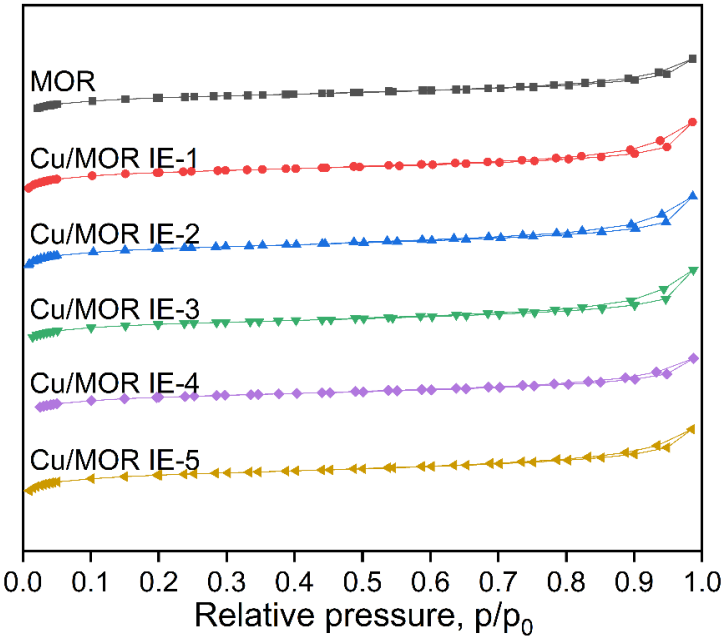

Figure S4. Nitrogen adsorption-desorption isotherms obtained at 77K for Cu/MOR samples.

S8. HRTEM

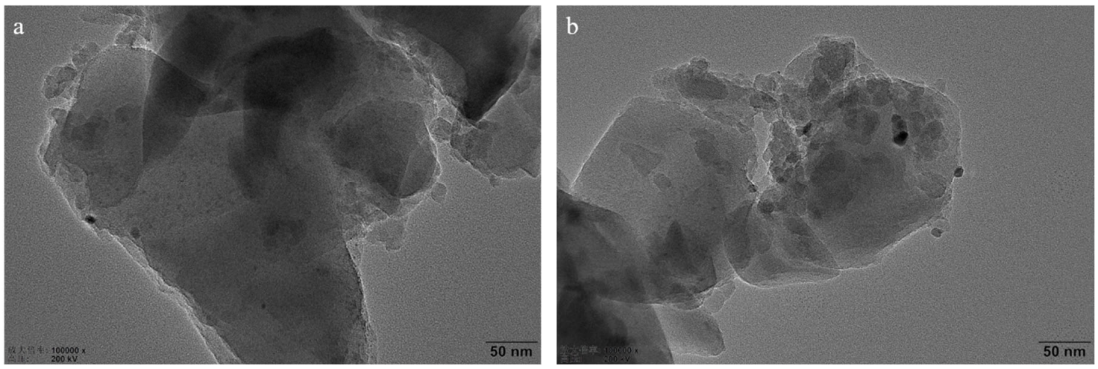

Figure S5. HRTEM patterns of (a) fresh Cu/MOR IE-4 catalyst and (b) spent Cu/MOR IE-4 catalyst.

High resolution transmission electron microscopy (HRTEM) was performed on JEM-2100F with an accelerating voltage of 200 kV. As shown in Figure S5, there are no evident copper particles on the Cu/MOR surface.

S9. NH_3-TPD

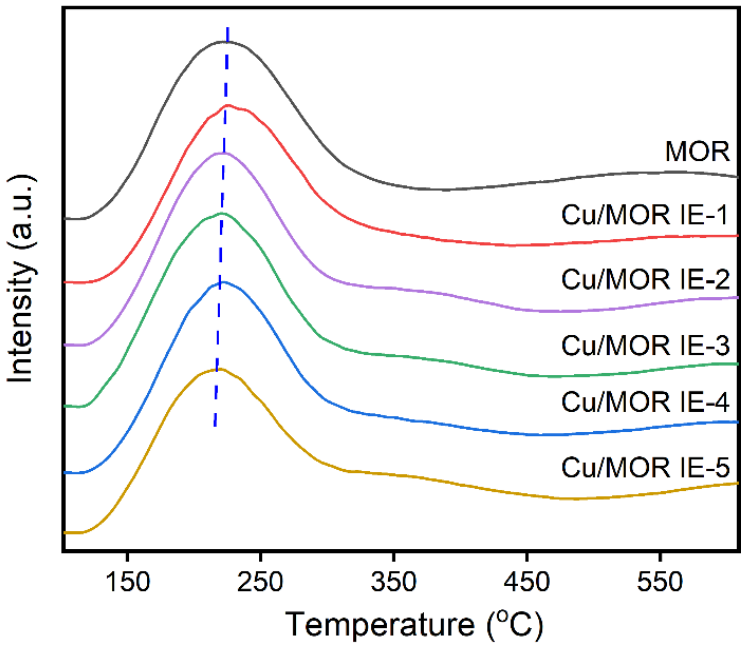

Figure S6. NH_3-TPD patterns of the fresh Cu/MOR catalysts with different exchange levels.

The acidity of the MOR and Cu-MOR samples was measured by NH_3 temperature programmed desorption (NH_3-TPD) and infrared spectroscopy of pyridine adsorption (Py-IR). The NH_3-TPD profile (Figure S6) shows simple MOR zeolites desorbing NH_3 in two different temperature ranges: a low temperature desorption range corresponding to weakly bound NH_3, and another high temperature range corresponding to relative strongly bound NH_3. The new desorption peak at around 320 °C after Cu ion exchange is attributed to NH_3 adsorption on sites of medium acidity, thus indicating the formation of new acidic sites, while strong acidic sites disappear and the central temperature of weak acidic sites shifts to lower temperatures, indicating weakening of the acidic strength.[11]

S10. Three experiments of Cu-MOR catalyst treated by different plasmas

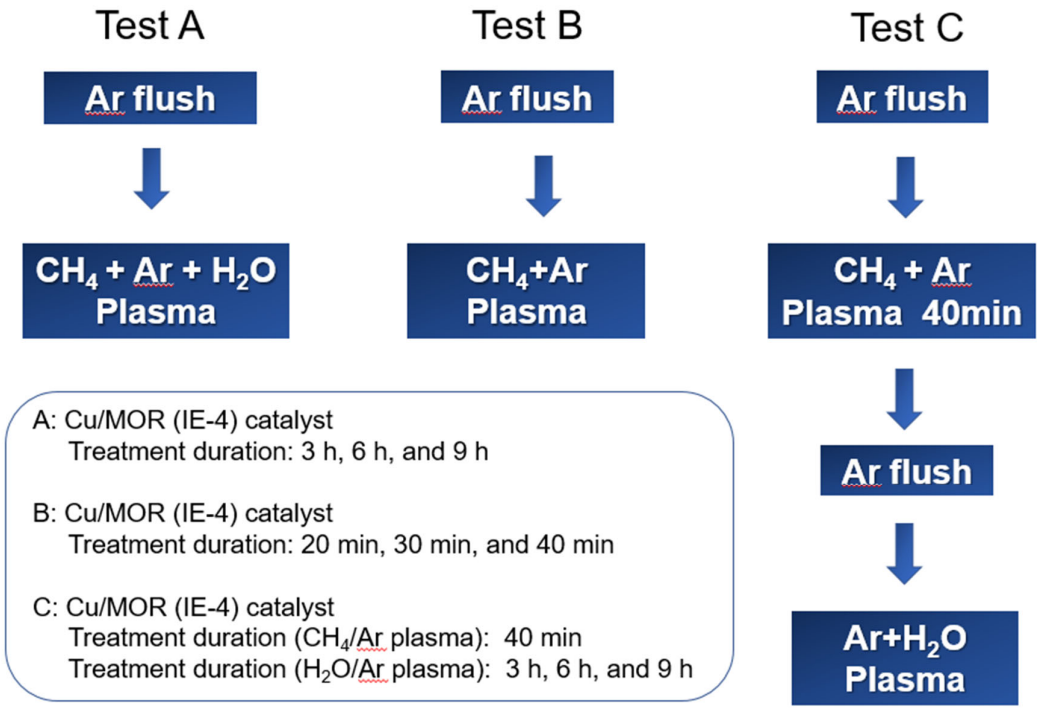

Figure S7. Diagram of Cu/MOR catalysts treated under different plasma conditions

S11. Lissajous plots under different conditions

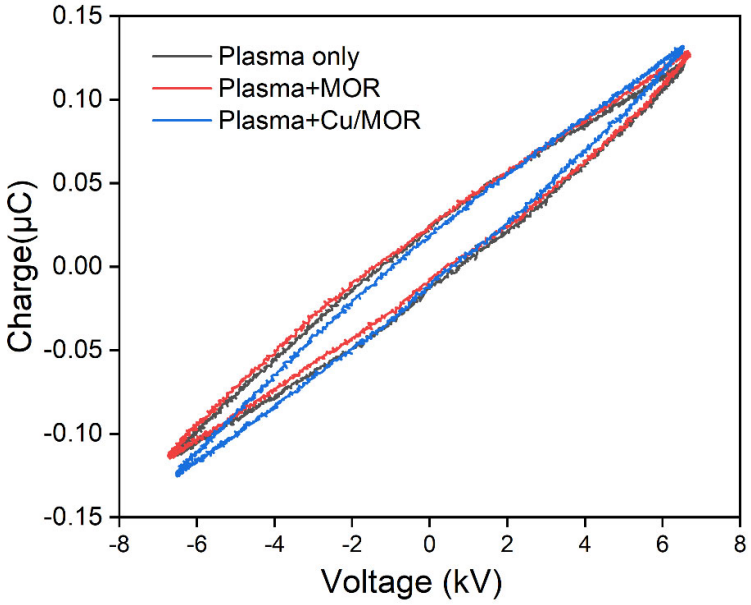

Figure S8. Lissajous plots for plasma only, plasma + MOR, and plasma + Cu/MOR at 443 K.

The Lissajous figures (Figure S8) of plasma, plasma + MOR and plasma + Cu/MOR were used to calculate the plasma power and monitor the discharge properties. There is no evident change in the Lissajous figures between plasma + MOR and plasma + Cu/MOR.

References

(1) Jeong, Y. R.; Jung, H.; Kang, J.; Han, J. W.; Park, E. D., Continuous synthesis of methanol from methane and steam over copper-mordenite. *ACS Catal.* **2021**, 11 (3), 1065-1070.

(2) Koishybay, A.; Shantz, D. F., Water is the oxygen source for methanol produced in partial oxidation of methane in a flow reactor over Cu-SSZ-13. *J. Am. Chem. Soc.* **2020**, 142, 11962-11966.

(3) Sun, L.; Wang, Y.; Wang, C.; Xie, Z.; Guan, N.; Li, L., Water-involved methane-selective catalytic oxidation by dioxygen over copper zeolites. *Chem* **2021**, 7, 1557-1568.

(4) Lee, S. H.; Kang, J. K.; Park, E. D., Continuous methanol synthesis directly from methane and steam over Cu(II)-exchanged mordenite. *Korean J. of Chem. Eng.* **2018**, 35, 2145-2149.

(5) Sushkevich, V. L.; Palagin, D.; Ranocchiari, M.; van Bokhoven, J. A., Selective anaerobic oxidation of methane enables direct synthesis of methanol. *Science* **2017**, 356, 523–527.

(6) Sushkevich, V. L.; Palagin, D.; van Bokhoven, J. A., The effect of the active-site structure on the activity of copper mordenite in the aerobic and anaerobic conversion of methane into methanol. *Angew. Chem. Int. Ed.* **2018**, 57, 8906-8910.

(7) Takayuki., T.; Iizuka, S., Conversion of methane to methanol by a low-pressure steam plasma. *J. Environ. Eng. Technol* **2013**, 2, 35-39.

(8) Okazaki, K.; Kishida, T.; Ogawa, K.; Nozaki, T., Direct conversion from methane to methanol for high efficiency energy system with exergy regeneration. *Energy Conv. Manag.* **2002**, 43, 1459–1468.

(9) Bi, W.; Tang, Y.; Li, X.; Dai, C.; Song, C.; Guo, X.; Ma, X., One-step direct conversion of methane to methanol with water in non-thermal plasma. *Commun. Chem.* **2022**, 5, 124.

(10) Tang, Y.; Cui, Y.; Ren, G.; Ma, K.; Ma, X.; Dai, C.; Song, C., One-step synthesis methanol and hydrogen of methanol and hydrogen from methane and water using non-thermal plasma and Cu-Mordenite catalyst. *Fuel Process. Technol.* **2023**, 224, 107722.

(11) Wang, S.; Guo, W.; Zhu, L.; Wang, H.; Qiu, K.; Cen, K., Methyl acetate synthesis from dimethyl ether carbonylation over mordenite modified by cation exchange. *J. Phys. Chem. C* **2014**, 119, 524-533.